CHAPTER IV
RESULTS AND DISCUSSION

For better understanding of the chemical reactions in a plasma environment, the possibilities of chemical pathways, which occurred by the collisions between electrons and all reactants in order to produce H_2 and various hydrocarbon species, were shown as the following reactions (Pornmai *et al.*, 2012);

Electron-carbon dioxide collisions:

$$e^- + CO_2 \rightarrow CO + O^- \quad (13)$$

$$e^- + CO_2 \rightarrow CO + O + e^- \quad (14)$$

$$e^- + CO \rightarrow C + O + e^- \quad (15)$$

Electron-methane collisions:

$$e^- + CH_4 \rightarrow CH_3 + H + e^- \quad (16)$$

$$e^- + CH_3 \rightarrow CH_2 + H + e^- \quad (17)$$

$$e^- + CH_2 \rightarrow CH + H + e^- \quad (18)$$

$$e^- + CH \rightarrow C + H + e^- \quad (19)$$

$$H + H \rightarrow H_2 \quad (20)$$

Electron-ethane collisions:

$$e^- + C_2H_6 \rightarrow C_2H_5 + H + e^- \quad (21)$$

$$e^- + C_2H_5 \rightarrow C_2H_4 + H + e^- \quad (22)$$

$$e^- + C_2H_4 \rightarrow C_2H_3 + H + e\text{-} \quad (23)$$

$$e^- + C_2H_3 \rightarrow C_2H_2 + H + e^- \quad (24)$$

$$e^- + C_2H_6 \rightarrow CH_3 + CH_3 + e^- \quad (25)$$

Electron-propane collisions:

$$e^- + C_3H_8 \rightarrow C_3H_7 + H + e^- \quad (26)$$

$$e^- + C_3H_7 \rightarrow C_3H_6 + H + e^- \quad (27)$$

$$e^- + C_3H_8 \rightarrow C_2H_5 + CH_3 + e^- \quad (28)$$

Electron-water collisions:

$$e^- + H_2O \rightarrow O^- + 2H \quad (29)$$

$$e^- + H_2O \rightarrow OH^- + H \quad (30)$$

Under the presence of oxygen, several chemical reactions can be initiated in the plasma environment as follows:

Dissociative attachment:

$e^- + O_2 \rightarrow 2O^- + e^- \rightarrow O^- + O$ (31)

$e^- + O_2 \rightarrow O_2^-$ (32)

$e^- + O_2 \rightarrow 2O^- + e^-$ (33)

Oxidative dehydrogenation reactions:

$CH_4 + O\ (O^-, O_2^-) \rightarrow CH_3 + OH\ (OH^-, HO_2^-)$ (34)

$C_2H_6 + O\ (O^-, O_2^-) \rightarrow C_2H_5 + OH\ (OH^-, HO_2^-)$ (35)

$C_2H_5 + O\ (O^-, O_2^-) \rightarrow C_2H_4 + OH\ (OH^-, HO_2^-)$ (36)

$C_2H_4 + O\ (O^-, O_2^-) \rightarrow C_2H_3 + OH\ (OH^-, HO_2^-)$ (37)

$C_2H_3 + O\ (O^-, O_2^-) \rightarrow C_2H_2 + OH\ (OH^-, HO_2^-)$ (38)

$C_3H_8 + O\ (O^-, O_2^-) \rightarrow C_3H_7 + OH\ (OH^-, HO_2^-)$ (39)

$C_3H_7 + O\ (O^-, O_2^-) \rightarrow C_3H_6 + OH\ (OH^-, HO_2^-)$ (40)

$CH_4 + OH\ (O^-, O_2^-) \rightarrow CH_3 + H_2O\ (OH^-, HO_2^-)$ (41)

$C_2H_6 + OH\ (O^-, O_2^-) \rightarrow C_2H_5 + H_2O\ (OH^-, HO_2^-)$ (42)

$C_2H_5 + OH\ (O^-, O_2^-) \rightarrow C_2H_4 + H_2O\ (OH^-, HO_2^-)$ (43)

$C_2H_4 + OH\ (O^-, O_2^-) \rightarrow C_2H_3 + H_2O\ (OH^-, HO_2^-)$ (44)

$C_2H_3 + OH\ (O^-, O_2^-) \rightarrow C_2H_2 + H_2O\ (OH^-, HO_2^-)$ (45)

$C_3H_8 + OH\ (O^-, O_2^-) \rightarrow C_3H_7 + H_2O\ (OH^-, HO_2^-)$ (46)

$C_3H_7 + OH\ (O^-, O_2^-) \rightarrow C_3H_6 + H_2O\ (OH^-, HO_2^-)$ (47)

All the active species formed from either electron collisions and oxidative reactions can further react to form various products as follows:

Coupling reactions of active species:

Ethylene (C_2H_4) formation:

$CH_2 + CH_2 \rightarrow C_2H_4$ (48)

$CH_3 + CH_3 \rightarrow C_2H_4 + H_2$ (49)

$C_2H_5 + H \rightarrow C_2H_4 + H_2$ (50)

$C_3H_7 + H \rightarrow C_2H_4 + CH_4$ (51)

Propylene (C_3H_6) formation:

$C_2H_3 + CH_3 \rightarrow C_3H_6$ (52)

$C_2H_4 + CH_3 \rightarrow C_3H_6 + H$ (53)

$C_2H_5 + CH_3 \rightarrow C_3H_6 + H_2$ (54)

$C_2H_4 + CH_2 \rightarrow C_3H_6$ (55)

$C_2H_5^{\cdot} + CH_2^{\cdot} \rightarrow C_3H_6 + H^{\cdot}$ (56)

$C_2H_6 + CH_2^{\cdot} \rightarrow C_3H_6 + H_2$ (57)

Butane (C_4H_{10}) formation:

$C_2H_5 + C_2H_5 \rightarrow C_4H_{10}$ (58)

$C_3H_7 + CH_3 \rightarrow C_4H_{10}$ (59)

Carbonmonoxide (CO) formation

$CH_3 + O \rightarrow HCHO + H$ (60)

$HCHO + O \rightarrow OH + CHO$ (61)

$CHO + O \rightarrow OH + CO$ (62)

$CHO + OH \rightarrow CO + H_2O$ (63)

$CHO + H \rightarrow CO + H_2$ (64)

4.1 The Effects of Input Voltage

Input voltage is one of the important key parameters for plasma reforming. Here, the effects of input voltage were investigated by varying between 6.6-21 kV. The experiment was started at 6.6 kV due to the breakdown voltage and ended with at 21 kV due to the instability of plasma to spark discharge. Other parameters were kept constant at frequency of 300 Hz, flow rate of 100 cm^3/min and electrode gap distance of 10 mm, respectively. In addition from the previous work, the optimum hydrocarbons to oxygen feed molar ratio was 2:1 (Pornmai *et al.*, 2012), so this condition would be used for all experiments.

4.1.1 The Effects of Input Voltage on Reactant Conversions and Product Yields

Figure 4.1 shows the results of reactant conversions with various input voltage. It was found that the reactant conversions increased with increasing an input voltage. The increase of reactant conversions resulted from an increase of available electrons to initiate the plasma reactions with referring to more opportunities for collision. More available electrons were supported from an increase of generated current with increasing input voltage as shown in Figure 4.1c. The reactant conversions were in the following order of $C_3H_8 > C_2H_6 > CH_4 > CO_2$ resulting from

the bond dissociation energy of each element in the following order of 4.33, 4.35, 4.55 and 5.52 eV, respectively. Higher bond dissociation energy means to be dissociated more difficultly. In addition, CO_2 and CH_4 conversions slightly deceased after 15 kV due to a firstly changing of plasma characteristic to spark discharge which is unstable type of corona discharge. Especially on CO_2 conversion, a decrease of CO_2 conversion resulted from the increase of side reaction which was CO_2 formation via complete combustion with increasing input voltage (Pornmai *et al.*, 2012). The same results were found in product yields with increasing input voltage.

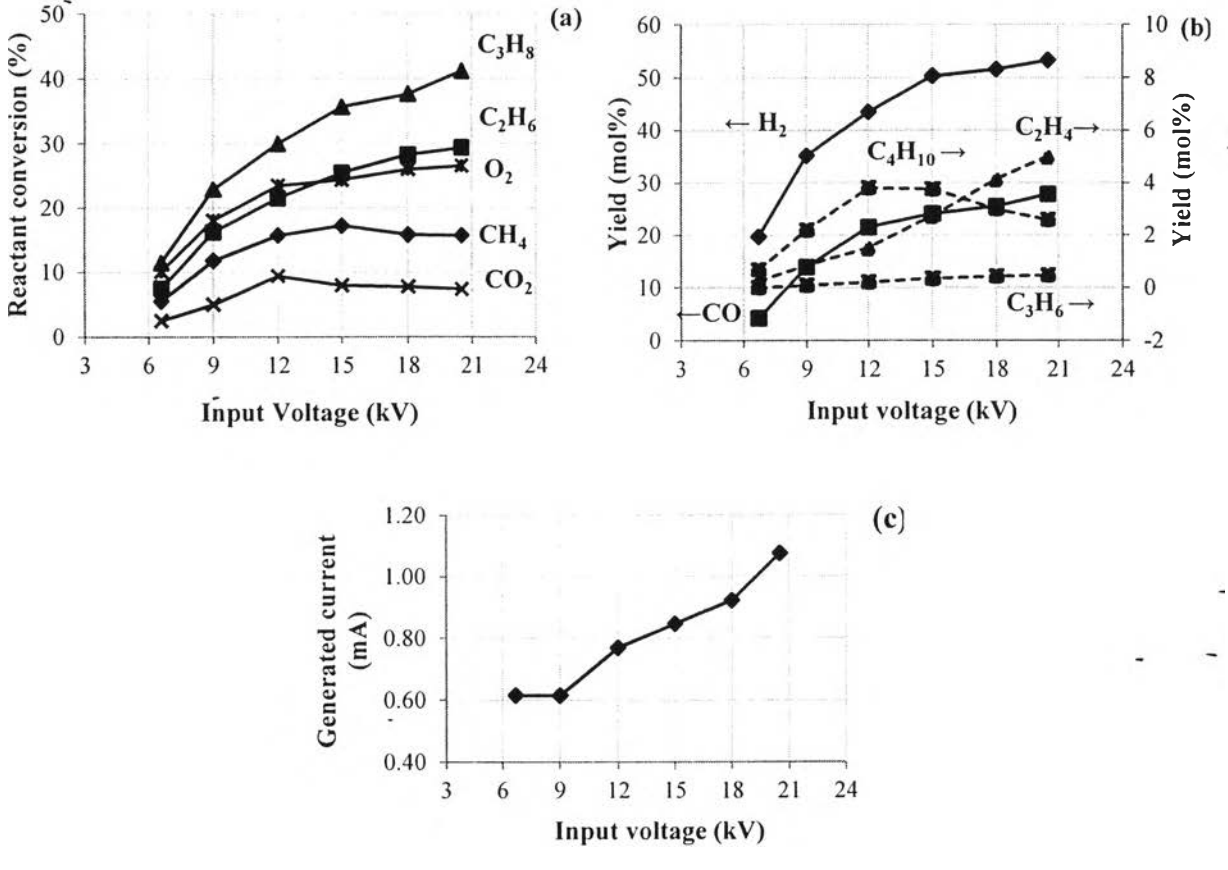

Figure 4.1 The effects of input voltage on reactant conversions (a), product yields (b) and generated current (c).

4.1.2 The Effects of Input Voltage on Product Selectivities

Figure 4.2 shows the effects of input voltage on product selectivites. The main products were H_2 and CO and other products of C_2H_4, C_3H_6 and C_4H_{10}. The H_2 selectivity sharply suppressed with increasing input voltage. The increase of electrons density resulted in more collision opportunities to from oxygen radicals for the oxidative dehydrogenation reactions to other products (Eq.34-47). These results agreed well with the selectivities of C_2H_4 and C_3H_6 which all increased with increasing an input voltage. According to the increase of oxidative dehydrogenation reactions, these products would further form CO (Eq.60-64) which agreed with the increase of CO selectivity. Another word, the increase of input voltage preferred the oxidative dehydrogenation reactions to the dehydrogenation reactions. The selectivities trend of H_2 and CO also agreed with a decrease of H_2/CO ratio with increasing input voltage. Moreover, the CO formation was possibly come from CO_2 dissociation. However, the high energy is required for CO_2 dissociation, so the CO formation would be dominated by the oxidative dehydrogenation reactions.

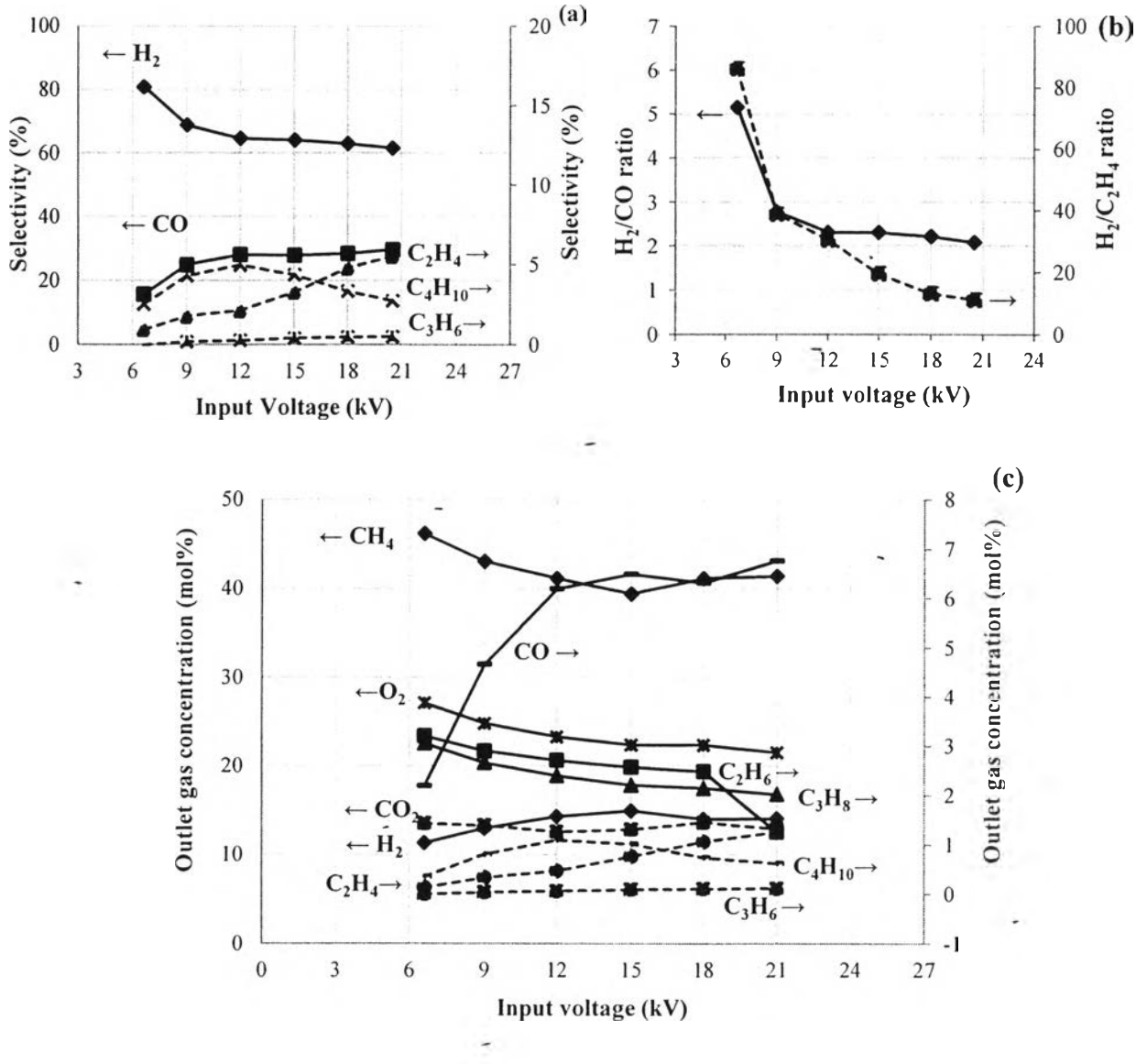

Figure 4.2 The effects of input voltage on product selectivities (a), ratio of H_2/CO, H_2/C_2H_4 (b) and outlet gas concentration (c).

4.1.3 The Effects of Input Voltage on Power Consumption and Coke Formation

Figure 4.3 shows the effects of input voltage on power consumption per reactant molecule converted and per H_2 molecule produced which significantly decreased with increasing input voltage from 6.6-15 kV resulting from the increase of reactant conversions and hydrogen yield. However, beyond 15 kV, power consumption started to increase which can be described by the decrease of CH_4 and CO_2

conversions. In addition, the change of plasma stability was observed with increasing input voltage beyond 15 kV. For coke formation, the results showed that coke formation increased with increasing input voltage. It can be implied that the increase of electron energy and density with increasing input voltage leaded to more collision, dissociation reaction and thermal cracking to produce coke. Another possibility explanation is the electron-carbon dioxide collisions as shown in Eq. 13-15. However, the high dissociation energy of CO was around 11.1 eV, so dissociation reaction and thermal cracking of other reactants were preferable for coke formation in the system.

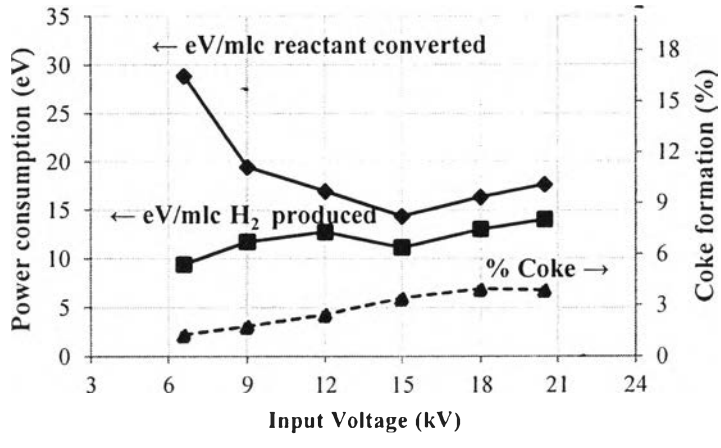

Figure 4.3 The effects of input voltage on power consumption and coke formation.

4.2 The Effects of Frequency

Frequency is also important parameter for plasma reforming which were observed from 300-600 Hz. The highest observed frequency was limited by the initial instability of plasma and the lowest observed frequency was also limited by plasma type to spark discharge. Input voltage was kept constant at 15 kV, which was the optimum voltage from the previous step. Other parameters also kept constant at a hydrocarbons to oxygen feed molar ratio at 2:1, feed flow rate at 100 cm^3/min and electrode gap distance at 10 mm.

4.2.1 The Effects of Frequency on Reactant Conversions and Product Yields

The effects of frequency on reactant conversions and product yields were presented in Figure 4.4. From the results, reactant conversions decreased with increasing frequency, excepted CO_2 conversion. In an AC system, the charges move in one direction in a very short time and reverse that direction which happens as a loop over the time. Frequency is described by this cycle of these switching directions. At higher frequency, it refers to faster reverse direction of charges resulting the decreased of current between 2 electrodes (Rader, 1997). In another word, an increase of frequency resulted in a decrease of current which agreed well with this experiment results (Figure4.4 (c)). According to the decrease of current, the number of electrons decreased resulting in lower collision opportunities and weaker electric field strength for initiating the plasma reactions. Consequently, almost reactants conversions and product yields decreased with increasing frequency. The opposite trend was found from CO_2-conversion that decreased with decreasing frequency due to an increase of the formation of carbon dioxide by complete combustion. These results can be implied that the electron-carbon dioxide collisions (Eq. 13-15) favored to occur at high frequency.

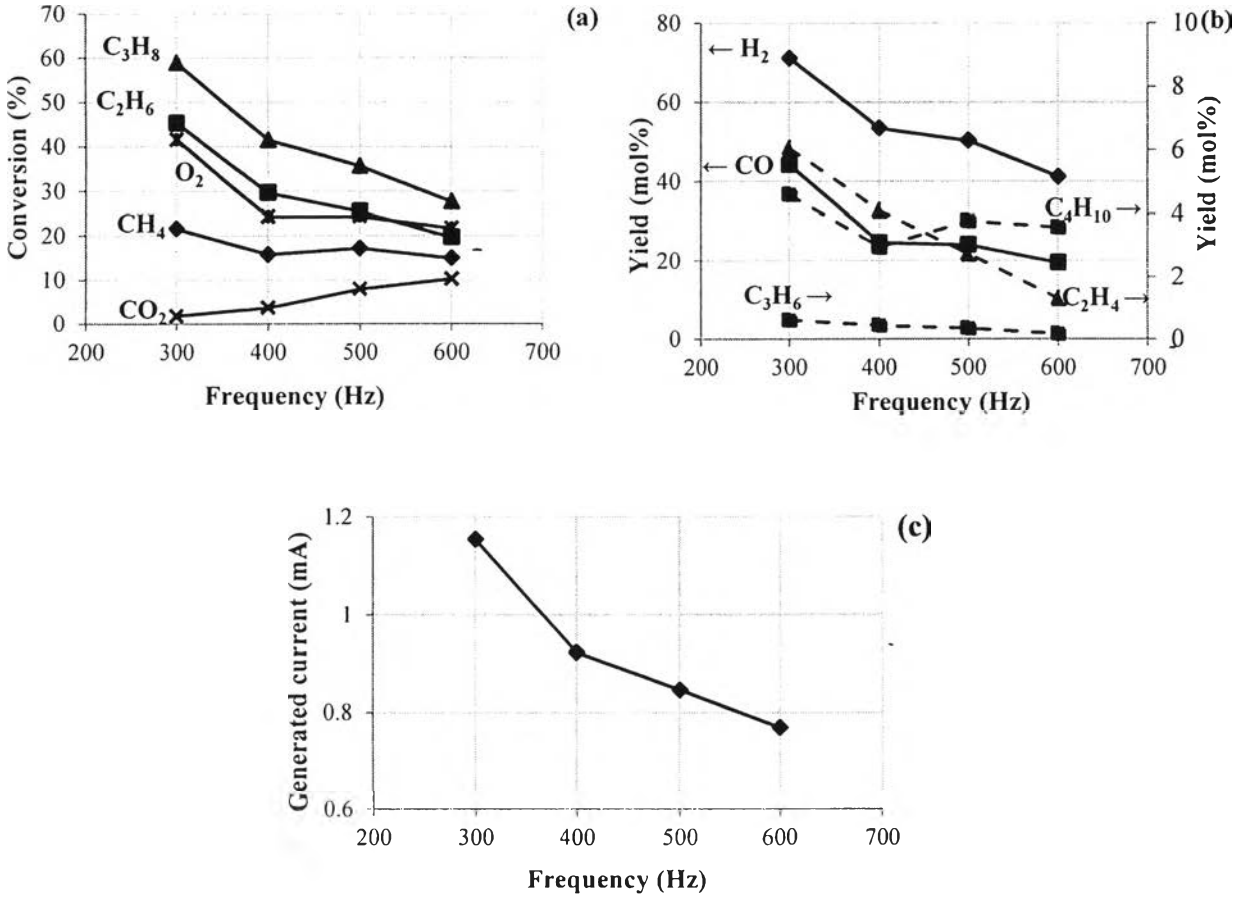

Figure 4.4 The effects of frequency on reactant conversions (a), product yields (b) and generated current (c).

4.2.2 The Effects of Frequency on Product Selectivities

The effects of frequency on product selectivities were presented in Figure 4.5. The results showed that the main products were H_2 and CO and following by C_2H_4, C_3H_6 and C_4H_{10}. The selectivity of H_2 decreased with decreasing frequency due to more providing oxygen radicals in the system. Hence, the oxidative dehydrogenation reactions (Eq. 34-47) are preferable to dehydrogenation (Eq. 16-28). This reason agrees well with the increase of CO, C_2H_4 and C_3H_6 when decreasing frequency. In generally, the formation of CO is possibly produced from the dissociation of CO_2 to CO (Eq. 13-15). However due to high dissociation energy

of CO_2, CO formation pathway was probably dominated by the oxidative dehydrogenation reactions from other reactants agreeing with the decrease of CO_2 conversion, meanwhile the CO selectivity and CH_4, C_2H_6, C_3H_8 conversion increased. The decrease of H_2/C_2H_4 and H_2/CO ratios with decreasing frequency also supported the dominated reaction of oxidative dehydrogenation instead of dehydrogenation to form H_2.

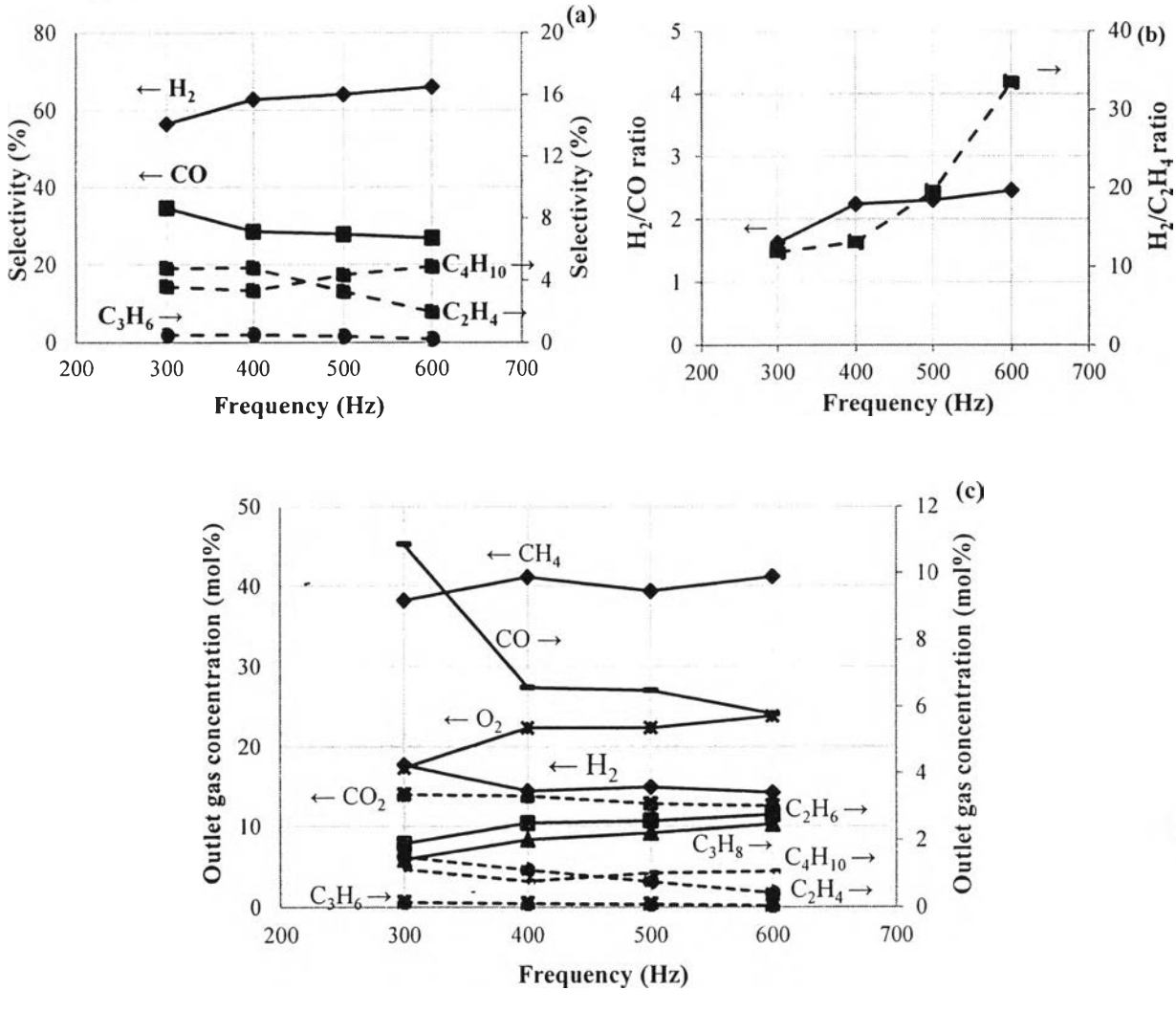

Figure 4.5 The effects of frequency on product selectivities (a),ratio of H_2/CO, H_2/C_2H_4 (b) and outlet gas concentration (c).

4.2.3 The Effects of Frequency on Power Consumption and Coke Formation

Figure 4.6 shows that the effects of frequency power consumption per reactant molecule converted and per H_2 molecule produced were significantly decreased with decreasing frequency due to the increase of CH_4, C_2H_6, C_3H_8 conversions and hydrogen yields. Coke formation increased with decreasing frequency from 600 to 500 Hz due to cracking process from more availability electrons in the system. However, coke formation started to decrease with decreasing frequency from 500-300 Hz. resulting from more oxygen radicals at low frequency which can possibly promote coke burning or complete combustion reaction.

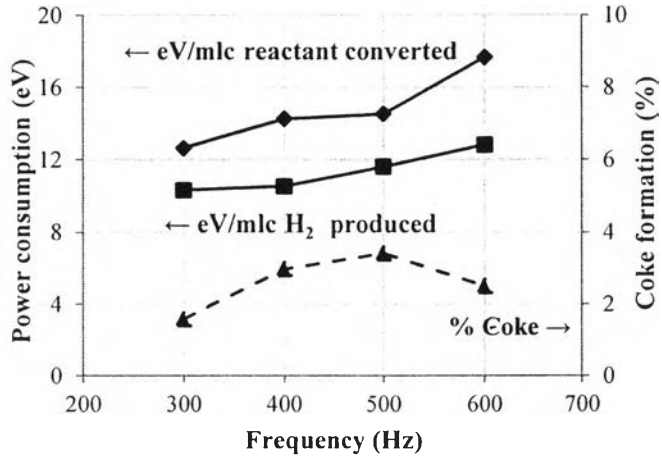

Figure 4.6 The effects of input voltage on power consumption and coke formation.

4.3 The Effect of Feed Flow Rate

The effects of feed flow rate were investigated in a range of 50 to 150 cm^3/min with keeping other parameters constant. Those are input voltage of 15 kV, frequency of 300 Hz with a hydrocarbons to oxygen feed molar ratio of 2:1 and electrode gap distance a 10 mm.

4.3.1 The Effect of Feed Flow Rate on Reactant Conversions and Product Yields

The effects of feed flow rate on conversions and yields were presented in Figure 4.7. The results showed that the reactant conversions and product yields decreased with increasing feed flow rate. The feed flow rate is directly related to residence time that the increase of feed flow rate means to the decrease of residence time resulting in less time for collision between charge particles in plasma. However, CO_2 conversion remains unchanged which can be implied that the total feed flow rate have insignificant effects on CO_2 conversion.

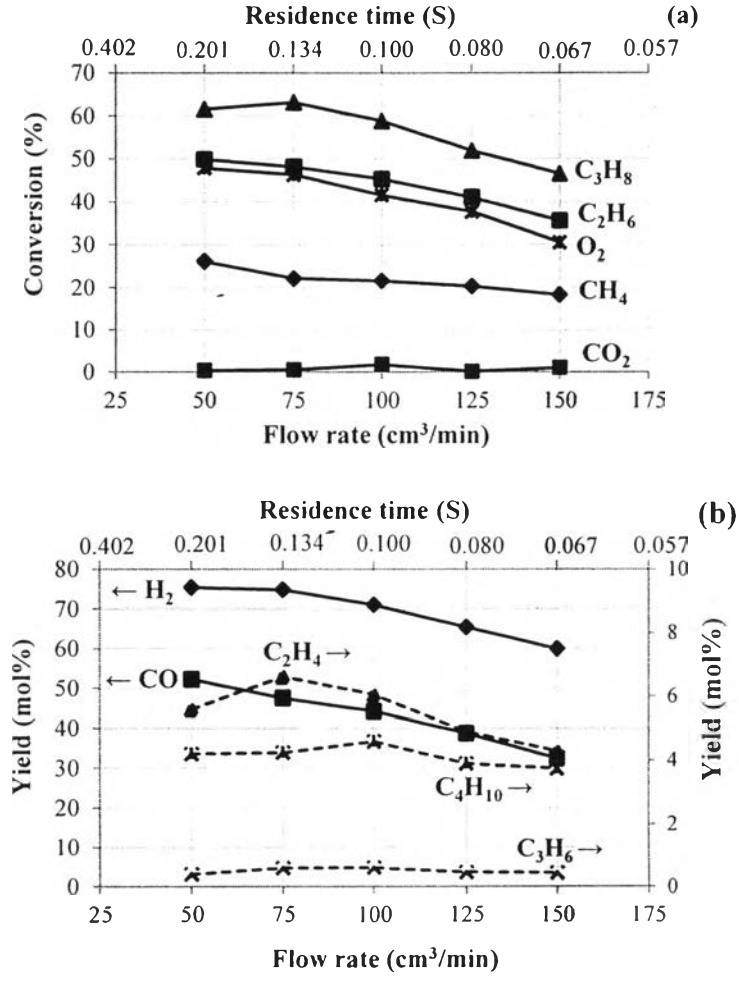

Figure 4.7 The effects of feed flow rate on reactant conversions (a) and product yields (b).

4.3.2 The Effect of Feed Flow Rate on Product Selectivities

The effects of feed flow rate on product selectivities were presented in Figure 4.8. The results showed that the main products were H_2 and CO with other products of C_2H_4, C_3H_6 and C_4H_{10}. The H_2 selectivity slightly decreased with decreasing feed flow rate, whereas the opposite trend was found in CO selectivity. According from the results, it is suggested that the oxidative dehydrogenation reactions preferably to occur with the increasing the retention time in plasma zone and respond to form CO. The decrease of H_2/C_2H_4 and H_2/CO ratios with decreasing feed flow rate also supported the dominated reaction of oxidative dehydrogenation. However, H_2/C_2H_4 ratio seems to increase again at 50 cm^3/min probably because long residence time caused C_2H_4 to form the larger molecule.

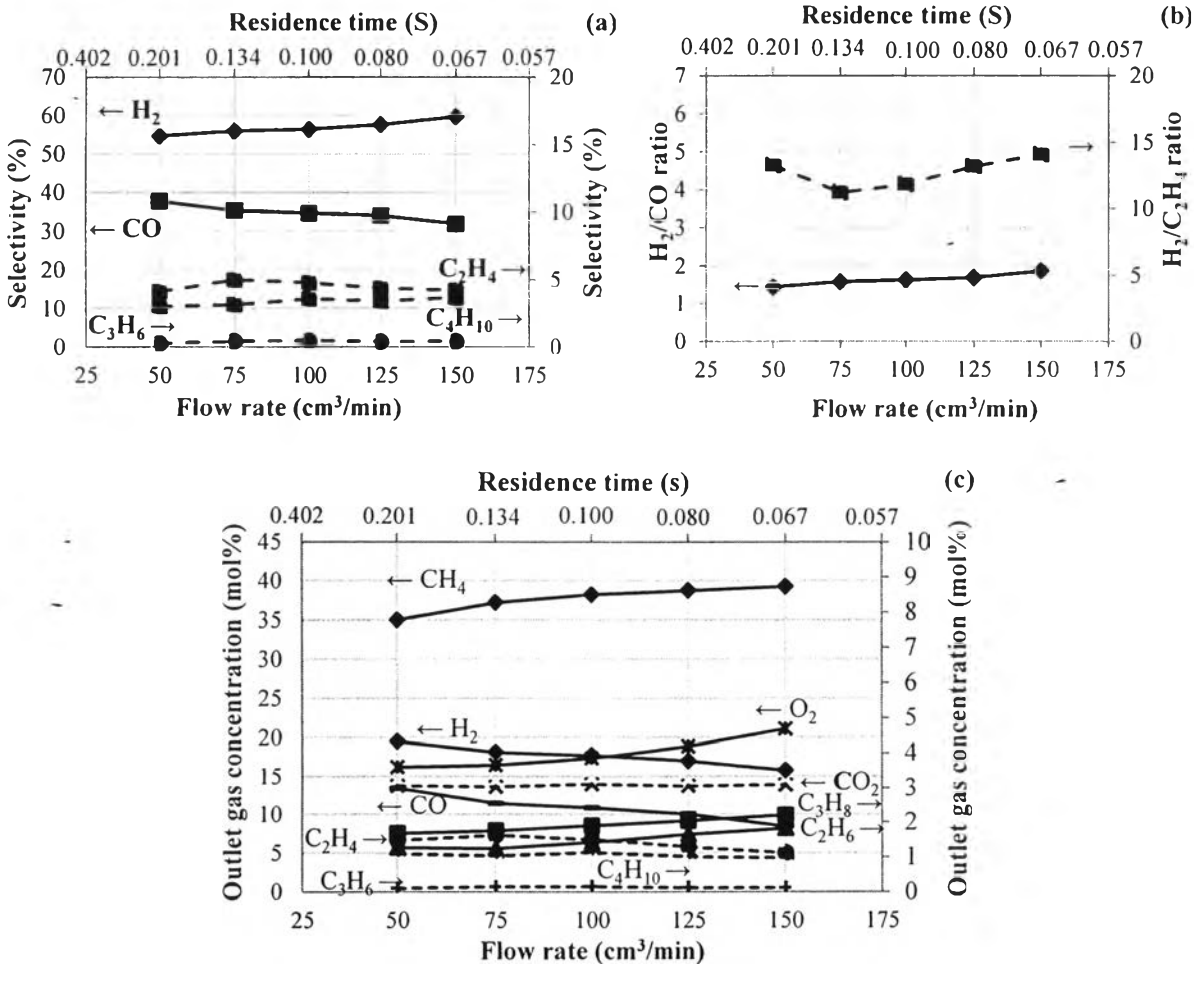

Figure 4.8 The effects of feed flow rate on product selectivities (a), ratio of H_2/CO, H_2/C_2H_4 (b) and outlet gas concentration (c).

4.3.3 The Effects of Feed Flow Rate on Power Consumption and Coke Formation

Figure 4.9 shows the effects of feed flow rate on power consumption. According to the increase in residence time, the higher CH_4, C_2H_6, C_3H_8 molecules converted as well as H_2 molecules produced. Consequently, power consumption per reactant molecule converted and per H_2 molecule produced was slightly decreased with decreasing feed flow rate. For coke formation, it seems slightly changing with varying feed flow rate.

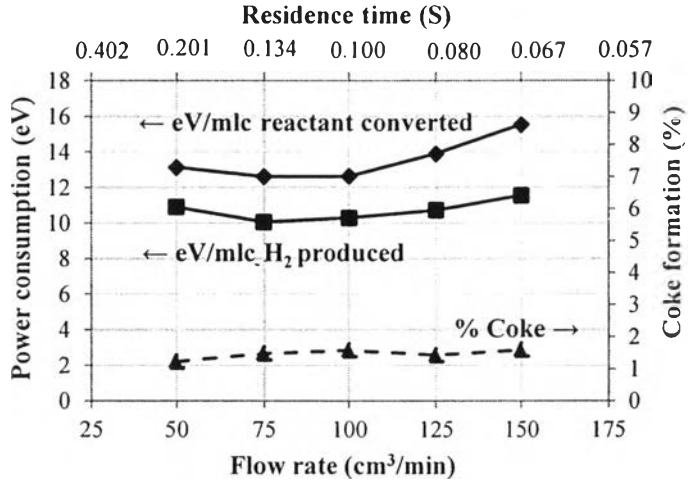

Figure 4.9 The effects of feed flow rate on power consumption and coke formation.

4.4 The Effects of Steam Addition

The effects of combined steam reforming and partial oxidation of natural gas at different steam conditions were carried out with a controlled temperature of 120 °C for preventing water condensation. The 4 different steam conditions were investigated, which were 5, 10, 15, 20 mol% of steam. The other parameters were kept constant from their optimum conditions at input voltage of 15 kV, frequency of 300 Hz and feed flow rate of 75 cm^3/min with a hydrocarbons to oxygen feed molar ratio of 2:1, and electrode gap distance 10 mm.

4.4.1 The Effects of Steam Addition on Reactant Conversions and Product Yields

The main function of steam addition was to provide O, OH radicals to initiate the plasma reactions. From Figure 4.10, the results showed that reactant conversions and product yields slightly increased with increasing mol% of steam from 0 to15 mol% resulting from abundant of oxygen radicals which had already been provided from the hydrocarbons to oxygen feed molar ratio at 2:1. Consequently, when steam was added in the system, there was slightly effect on the reactant conversions and product yields. The opposite trend was found in the oxygen conversion that slightly decreased with increasing mol% of steam. It is because there were oxygen radicals by the dissociation of steam resulting in competitive between oxygen and steam dissociation. In addition, the formation of oxygen by the collision of abundant oxygen radicals leaded to the decrease of O_2 conversion. At 20 mol% of steam, that reactant conversions and product yields decreased resulting from the plentiful of oxygen radicals which reduced the opportunities of collision between reactants and electrons (Supat *et al.*, 2003).

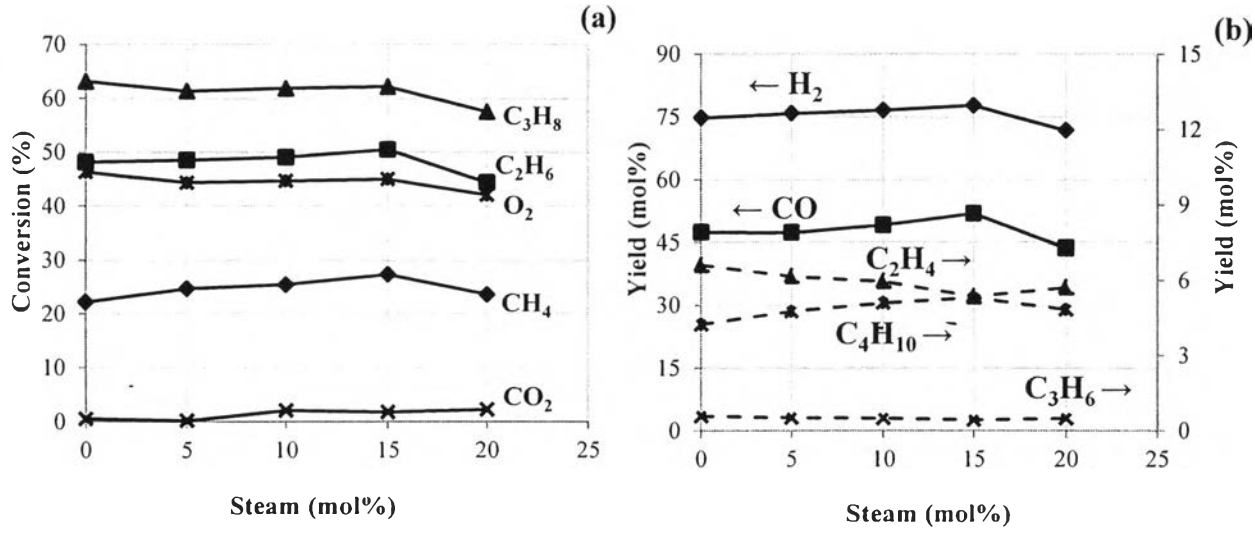

Figure 4.10 The effects of steam addition on reactant conversions (a) and product yields (b).

4.4.2 The Effect of Steam Addition on Product Selectivities

The effect of steam on product selectivity was shown in Figure 4.11 which the product selectivities slightly changed resulting from the abundant of oxygen in the system. The H_2 selectivity for 0-15 mol % of steam remained unchanged, whereas CO selectivity increased. It means that the oxidative dehydrogenation reactions were preferred to the dehydrogenation reactions. According unchanged H_2 selectivity, whereas the oxidative dehydrogenation reactions also dominated in the system resulting from the dehydrogenation of steam to form hydrogen instead of the dehydrogenation of other reactants which made the H_2/CO remain unchanged.

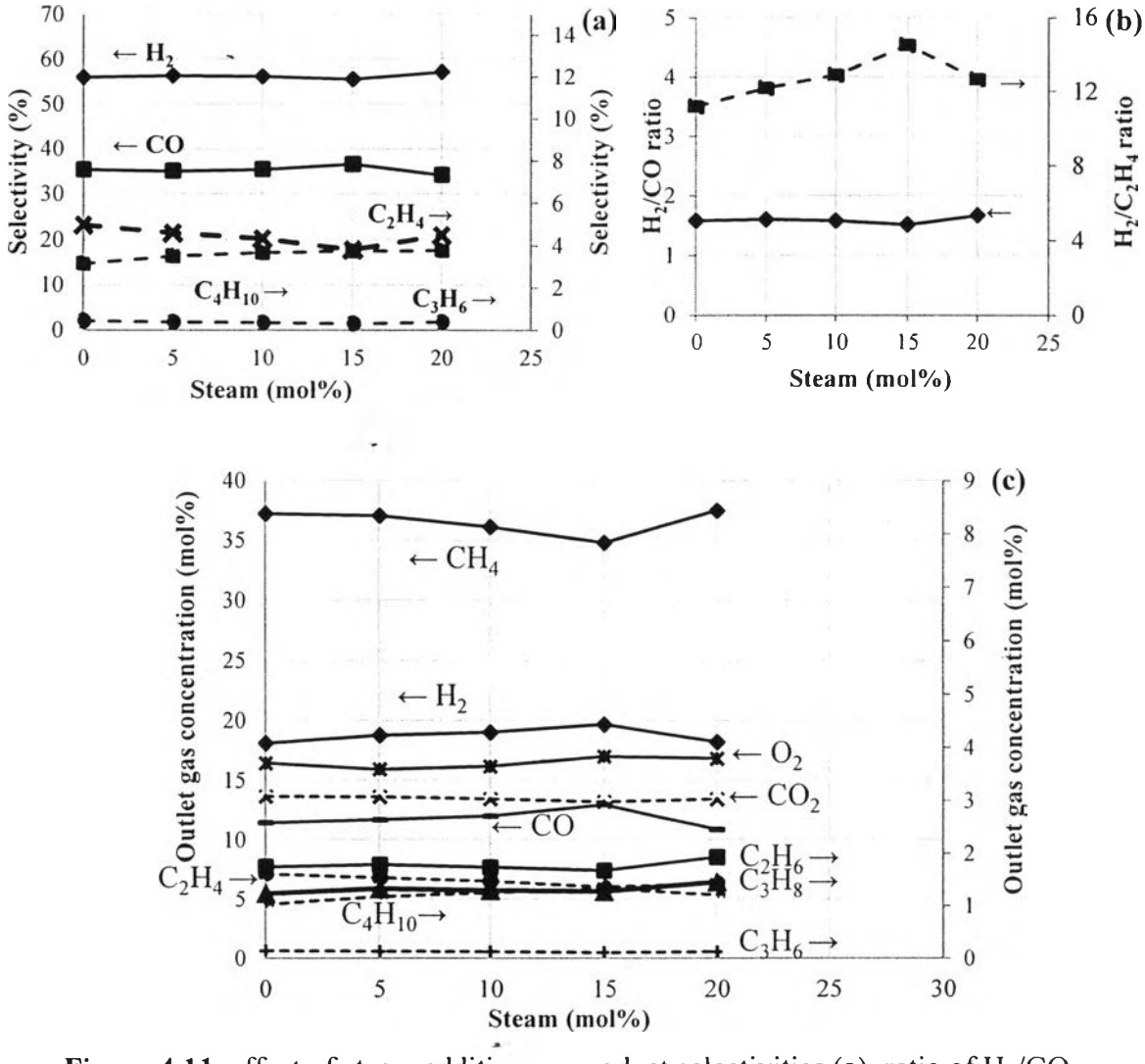

Figure 4.11 effect of steam addition on product selectivities (a), ratio of H_2/CO, H_2/C_2H_4 (b) and outlet gas concentration (c).

4.4.3 The Effects of Steam Addition on Power Consumption and Coke Formation

From Figure 4.12 shows the effects of steam on power consumption and coke formation. For power consumption, it decreased with increasing mol% of steam. Aforementioned that the roles of steam were to provide O/OH radicals for reactions, so it helps to initiate the reaction and be a H_2 source resulting in the decrease of power consumption. However at 20 mol% of steam, power consumption started to increase because of plentiful oxygen radicals resulting in a dilute in reactants concentration. From this reason, amount of converted reactants decreased following with a decrease in hydrogen produced. For coke formation, many researches proved that steam would help to decrease coke in the system. However, the coke slightly increased when steam was introduced into the system. It probably resulted from the increase of oxidative dehydrogenation which was preferable for the reactants cracking to form coke more than to enhance the production of other product by reacting with coke.

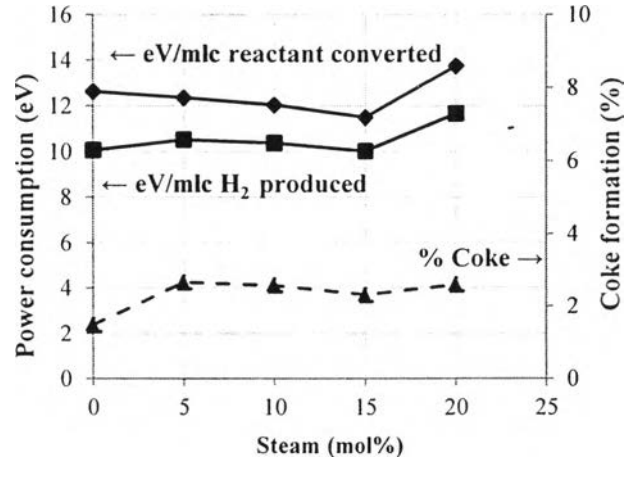

Figure 4.12 The effects of steam addition on power consumption and coke formation.

4.5 The Effects of Ni Catalysts on the Combined Steam Reforming with Partial Oxidation

Ni/Al_2O_3 catalysts with different Ni-loading were investigated. The total electrode gap distance between pin and plate was kept at 10 mm. The conditions in this step were kept from the previous steps which are hydrocarbons to oxygen feed molar ratio of 2:1, input voltage of 15 kV, frequency of 300 Hz, feed flow rate of 75 cm^3/min and steam of 15 mol%.

4.5.1 Catalyst Characterization

4.5.1.1 Atomic Absorption Spectroscopy

Table 4.1 The calculated and actual weight percentage of Ni loading

Calculated Ni loading (wt %)	Actual Ni loading (wt %)
5	5.03
7	6.51
10	10.9

4.5.1.2 X-ray Diffractometer

Figure 4.13 shows XRD patterns of different Ni loading. The XRD patterns presented the characteristic peaks of alumina at 2θ equal to 37.7, 46.0 and 67.0°. However, there were not characteristic peaks of any nickel species. It was suggested that high amount of Ni loading on the catalyst, which is typically more than 15 wt%, are required to observe the characteristic peaks (i.e. for NiO at 2θ 43.3, 63.0 and 79.5°) (Salagre *et al.*, 1996, Heracleous *et al.*, 2005, Maccarrone *et al.*, 2012). From Figure 4.14, the XRD patterns of the spent catalysts were detectable which can be implied that the crystalline of catalysts were not destroyed under the plasma environment. In addition, XRD pattern of 10 wt% Ni spent catalyst showed characteristic peak of NiO around 43.3° probably resulting from sintering effect to larger metal crystal until being possible to be detected.

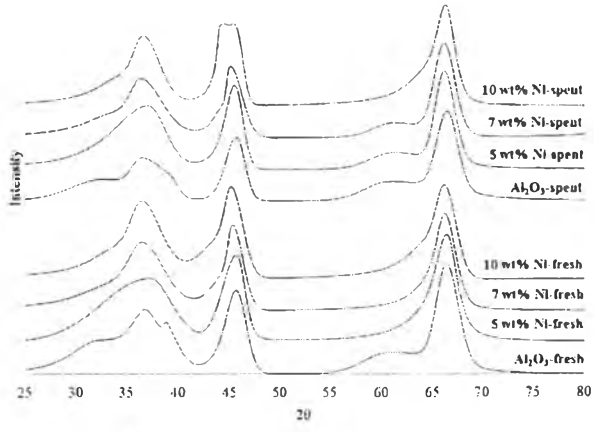

Figure 4.13 XRD patterns of Ni catalyst.

4.5.1.3 X-ray Photoelectron Spectroscopy

From Figure 4.14, narrow scan pattern of XPS on fresh catalysts showed the peak around 856.2 and 873.6 eV which corresponded to the splin-orbit line of Ni $2p_{3/2}$ and Ni $2p_{1/2}$. The peaks around 862.2 and 880 eV were the satellite structure of Ni $2p_{3/2}$ and Ni $2p_{1/2}$, respectively. The peak at 856.2 eV was deconvoluted into 2 peaks at binding energies of 854.2 and 856.2 eV which associated to the Ni $2p_{3/2}$ of NiO and Ni^{2+} of $NiAl_2O_4$, respectively (Jin *et al.*, 2000, Wang *et al.*, 2008). From XPS pattern, NiO seem to increase with increasing wt% of Ni loading. For XPS pattern of spent catalysts, XPS patterns showed only 2 species of Ni while Ni^0, which is an active species of methane reforming, do not exhibits. These results can be explained by the fact that, these systems were employed under excess of oxygen.

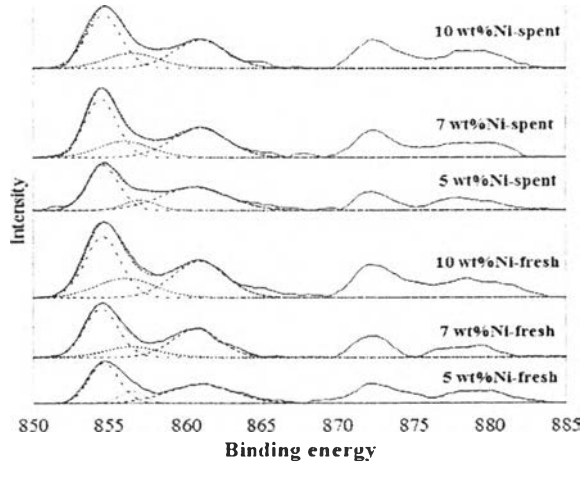

Figure 4.14 XPS patterns of Ni catalysts.

4.5.1.4 Surface Area Analyzer

Table 4.2 Surface area of Ni catalysts

	Al_2O_3	pelletized catalysts							
		Al_2O_3		5 wt% Ni		7 wt% Ni		10 wt% Ni	
surface area	262.5	F*	S*	F	S	F	S	F	S
(m^2/g)		242.6	224.3	217.6	213.6	202.6	187.3	198.8	172.5

Note: F* = Fresh catalyst and S* = Spent catalyst

Table 4.2 shows multiple point BET of each catalyst, surface area of fresh catalysts slightly decreased with increasing Ni loading resulting from the lower surface area of Ni which covered on Al_2O_3 support. For surface area of spent catalysts, surface area slightly decreased probably because this system was the combination of plasma and catalyst. Plasma might help to change the surface morphology which made the surface area of the catalysts slightly decreased by etching by plasma (Guo *et al.*, 2006).

4.5.1.5 Scanning Electron Microscopy

Figure 4.15 and Figure 4.16 shows SEM micrographs of Ni catalysts. From micrographs showed that the surface of spent catalyst had more roughness suface comparing with fresh catalysts. According to a slightly decrease of surface area, SEM micrographs confirmed that there were possibility that catalyst surface can be etched by plasma.

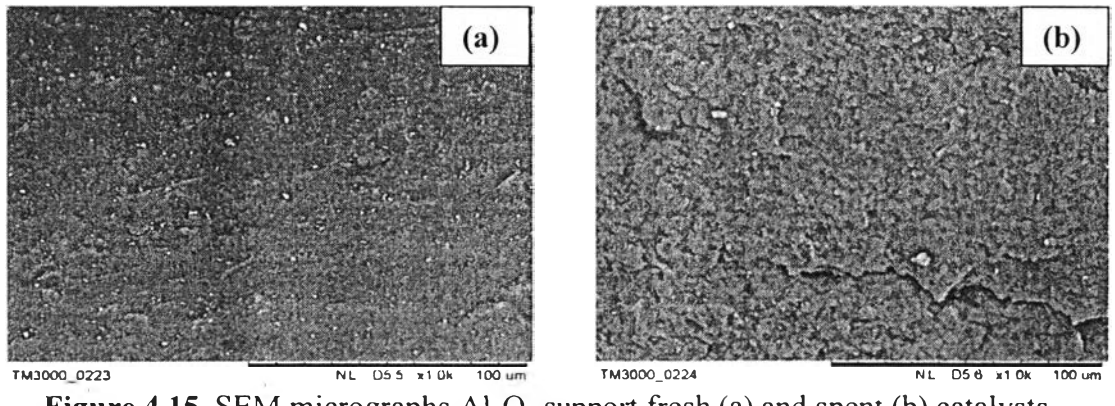

Figure 4.15 SEM micrographs Al_2O_3 support fresh (a) and spent (b) catalysts.

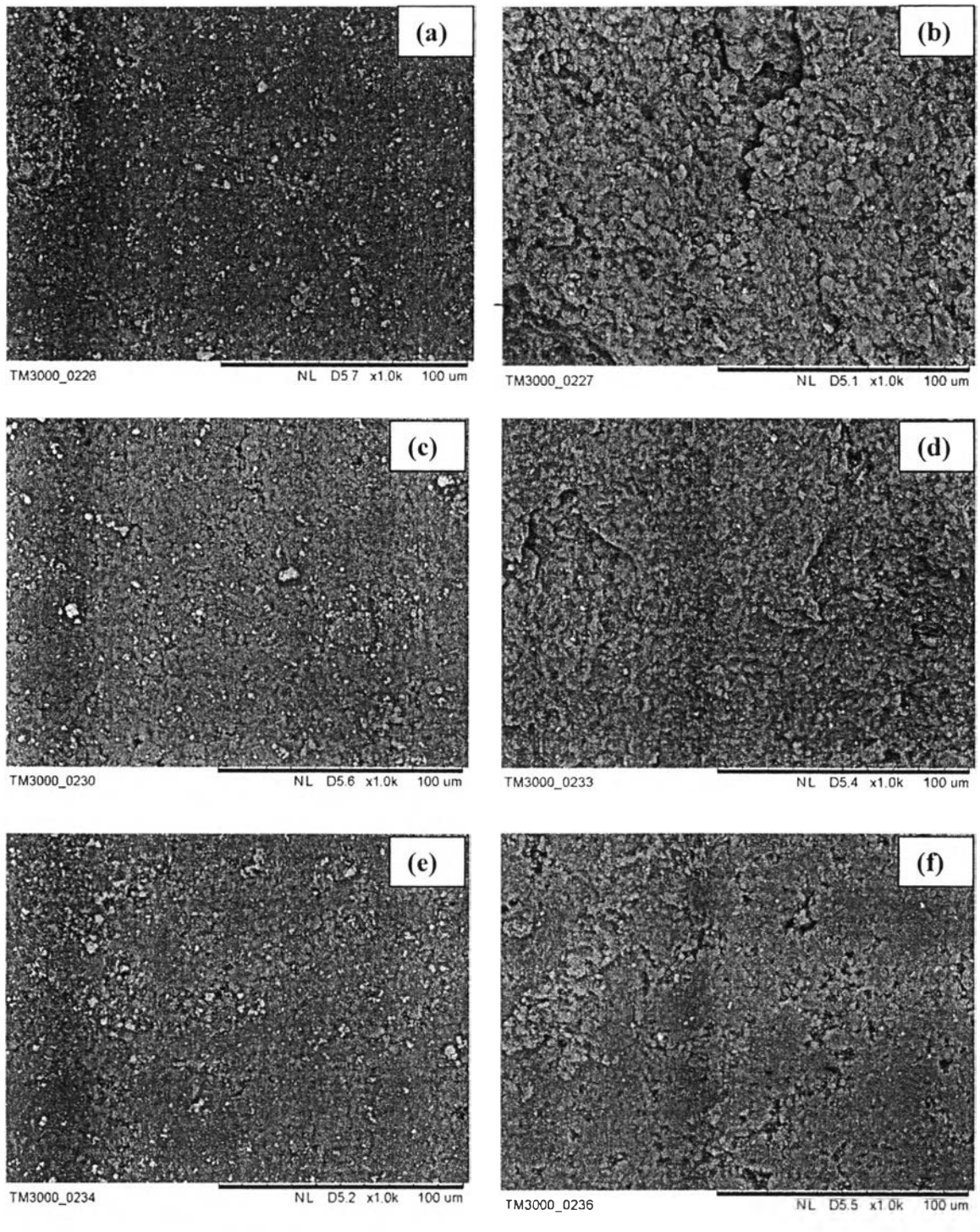

Figure 4.16 Set of SEM micrographs of fresh (a, c, e) and spent (b, d, f) Ni catalysts.

4.5.1.6 Temperature Program Oxidation

Table 4.3 shows the results of coke formation on the system. The results show that coke formation increased with increasing wt% of Ni loading. The mechanism of coke formation on Ni sides, it was suggested that natural gas would dissociate to monatomic carbon in order to further react and form CO. According to the increase of Ni sides with increasing wt% of Ni loading, it promoted the adsorption of reactant gases. However, the rate of reaction and desorption might take longer time and lead to accumulate of surface carbon following with the polymerization of carbon on the surface to coke (Zhu *et al.*, 2008). Figure 4.17 shows the TPO diagrams of spent catalysts. It was found that coke signals were around 400, 500 and 600 °C which correspond to soft and hard coke. For spent catalyst of Al_2O_3 support, only soft coke was found. However, the trends of coke shifted to hard coke when Ni was introduced into the system resulting from the carbon polymerization on the surface by the reactant adsorption on the Ni site.

Table 4.3 Percentage of coke formation on spent catalysts

	Al_2O_3	5 wt%Ni	7 wt%Ni	10 wt%Ni
Coke (wt%)	3.77	3.47	3.63	5.12

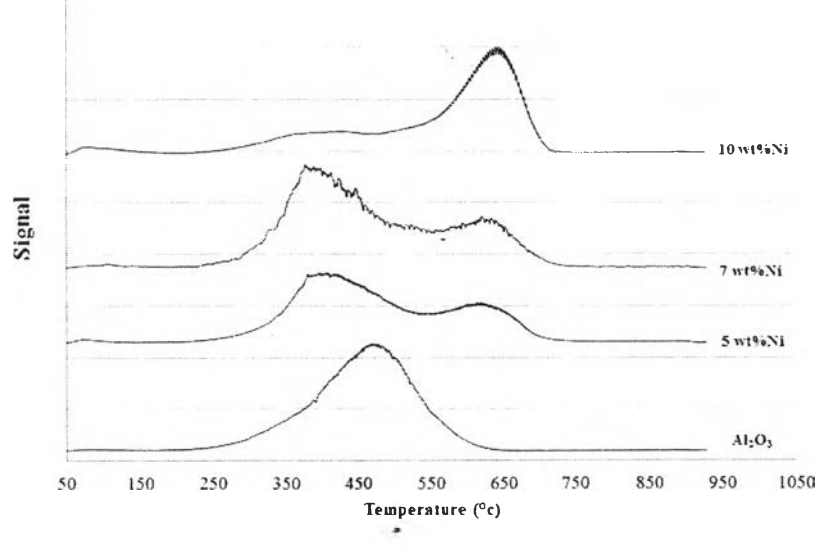

Figure 4.17 The TPO diagrams of spent catalyst.

4.5.2 The Effects of Ni Catalysts on Reactant Conversions and Product Yields

Figure 4.18 shows the reactant conversions and product yields.The experiment with Al_2O_3 support slightly increased reactant conversions resulting from the increase of the residence time in the plasma zone by adsorption on Al_2O_3support. According to longer time, the collision propability increased. Exspecially, CO_2 conversion increased which was promoted by adsorption and dissociation of CO_2 on catalysts (Durme *et al.*, 2008). For the differenceof Ni-loading catalysts, The results showed that reactant conversions increased with increasing wt% of Ni loading, whereas CO_2 conversion decreased with increasing wt% of Ni loading. The reason was longer residence time that reactants approached to plasma zone by adsorption on catalyst. Moreover, vibrationally excited species, which had too low internal energy to induce the reaction in gas phase, probably adsorbed on the catalyst surface and enchance the chemical reactions (Chen *et al.*, 2008). In generally, Ni^0 was suggested to be an active site to methane reforming reactions. Howerver, in this present work, oxygen was used as a reactant feed. Consequenctly, the NiO was considered as the main Ni species that the oxidation state of Ni was confirmed by XPS, as shown in Figure 4.14. Therefore, the reaction mechanism through NiO side probably followed by 2 steps mechanism. Firstly, hydrocarbons were oxidized to CO, CO_2 and H_2O resulting in reduction of NiO to Ni^0, following with CH_4 dissociation on Ni^0 to product H_2 (Jin *et al.*, 2000). Beside the hydrocarbon reactants, CO_2 coversion decreased remarkably with increasing wt% of Ni loading resulting from large amount of CO_2 formation from 1st step of mechanism, which couldn't further turn to CO, and complete combusion reaction by coke burning. The continiuous of CO_2 formation resulted in the decrease of the CO_2 coversion until getting negative at 10 wt% of Ni loading. For product yields, all product yields increased with increasing wt% of Ni loading. It should be note that over 100% of the H_2 yields was exhibited because the complex of the reactions consisted of 3 reactants and the selectivities were calculated base on dry basis without counting produced water.

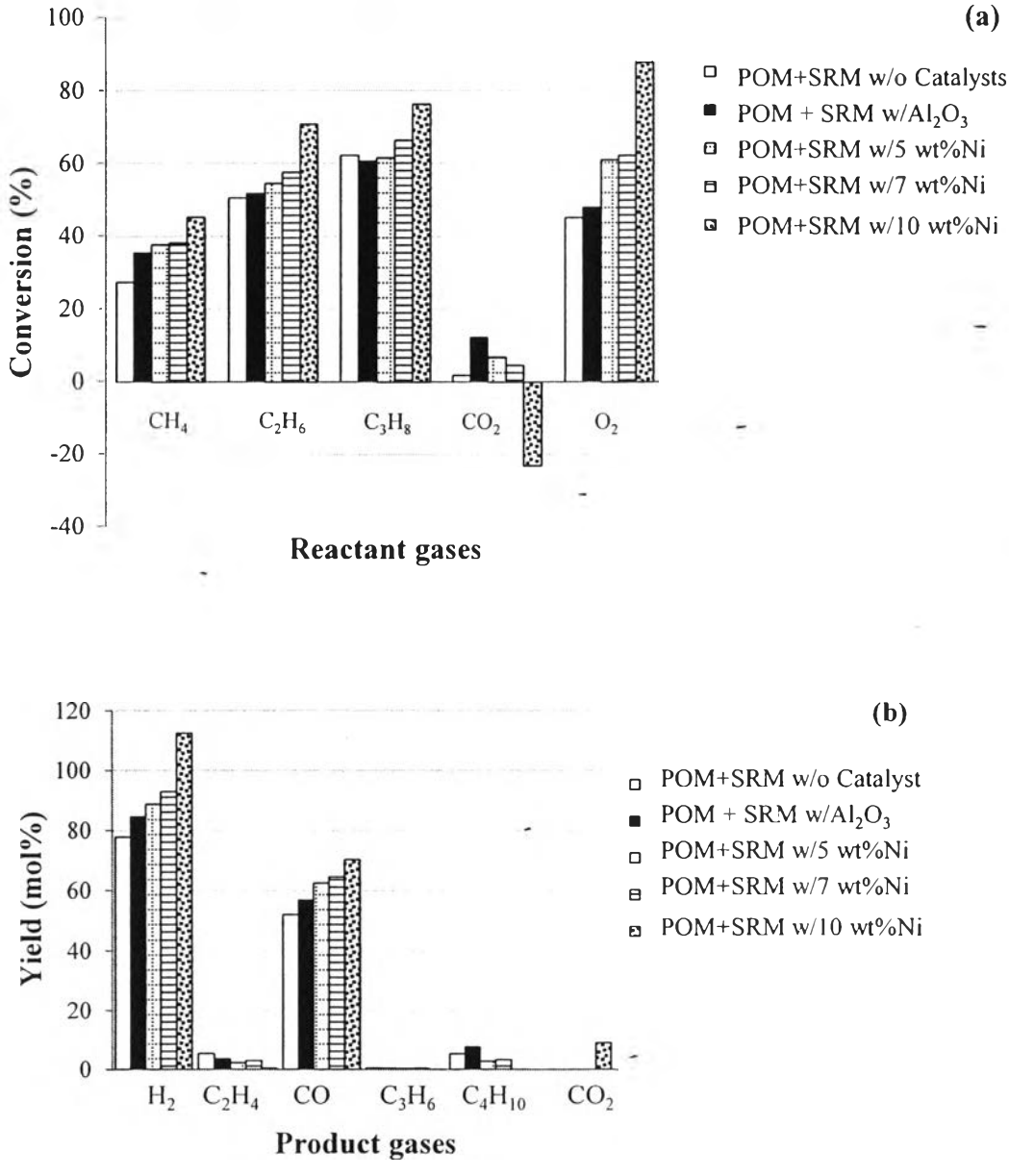

Figure 4.18 The effects of Ni catalysts on reactant conversions (a), product yields (b).

4.5.3 The Effects of Ni/Al_2O_3 Catalysts on Product Selectivities

Figure 4.19 shows the selectivities of product which the main products were synthesis gas. The H_2 selectivity slightly increased with increasing wt% of Ni loading and other hydrocarbon selectivities slightly decreased. Therefore, Ni catalysts possibly helped selecting to produce H_2 by the dissociation of other

hydrocarbon products. For CO selectivity, it firstly dropped for Al_2O_3resulting from the secondary reaction from CO_2 adsorption and radicals in gas phase to create other products, agree with a slightly increase of C_4H_{10}. When Ni catalyst was introduced, the CO selectivity firstly increased due to the presence of Ni catalysts in the system. However, the CO selectivity started to decrease again because of a decreasing in CO_2 conversion. For H_2/CO ratio, there was slightly changed in the presence of Ni catalysts.

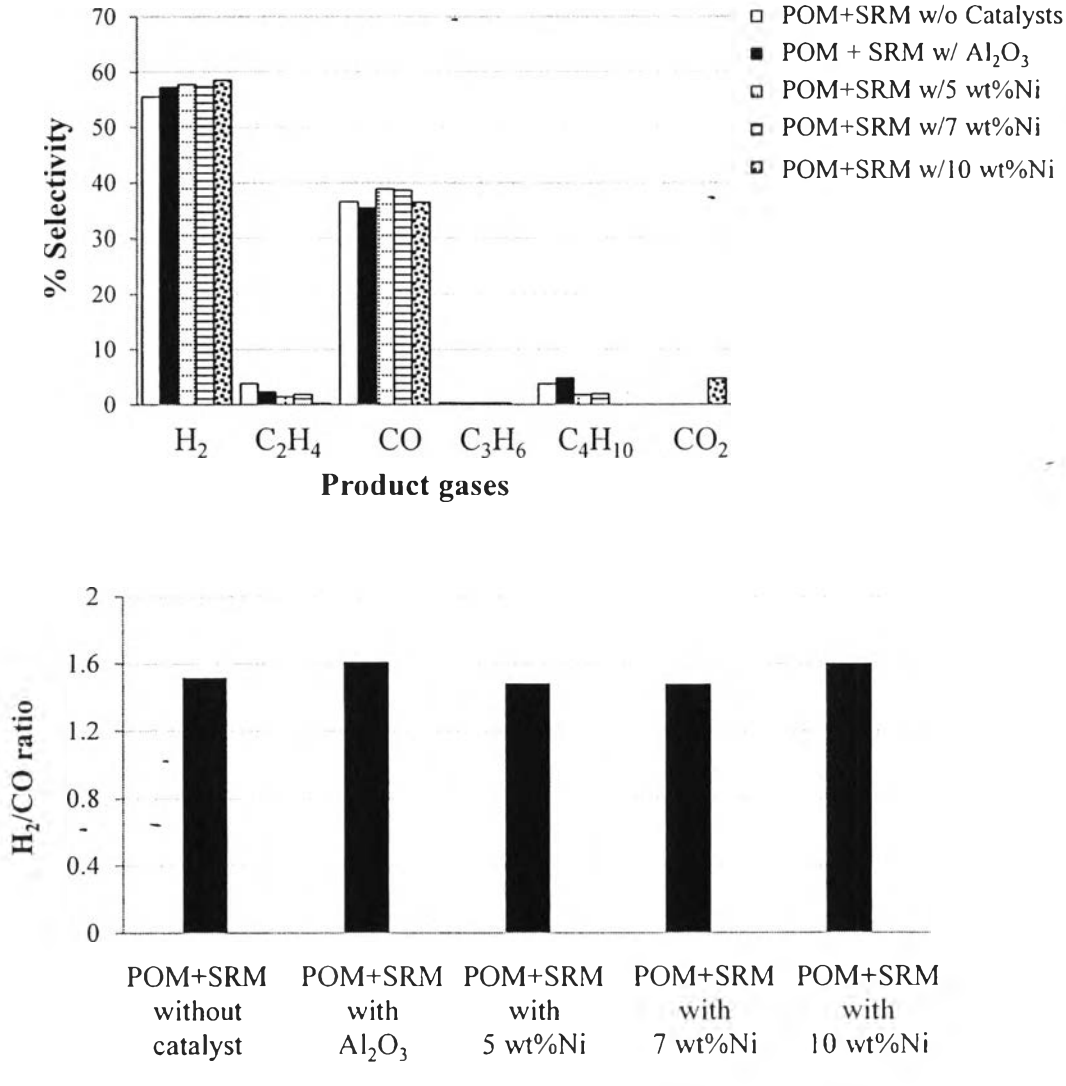

Figure 4.19 The effects of Ni catalysts on selectivities(a), ratio of H_2/CO ratio (b).

4.5.4 The Effects of Ni/Al_2O_3 Catalysts on Power Consumption

Figure 4.19 shows the effect of Ni catalysts on power consumption per reactant molecule converted and per H_2 molecule produced which significantly decreased with the presence of Ni catalysts resulting from an increase of reactant conversions and H_2 product because of the effect of plasma and catalysts.

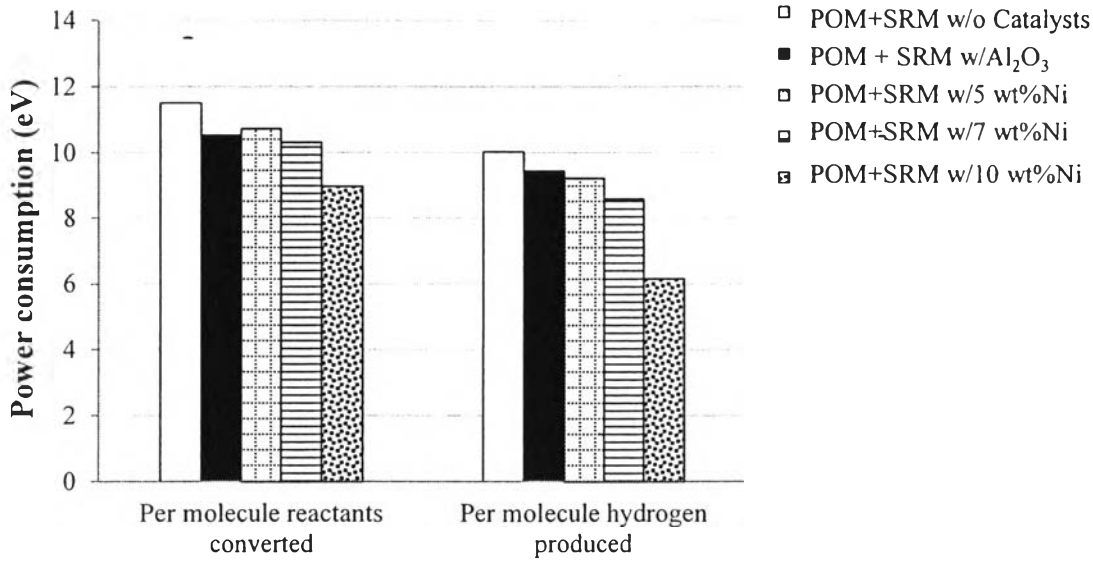

Figure 4.20 The effects of Ni catalysts on power consumption.